Contrib Mineral Petrol (2003) 146: 120–133
DOI 10.1007/s00410-003-0491-9

ORIGINAL PAPER

O. G. Safonov · Y. A. Litvin · L. L. Perchuk · L. Bindi
S. Menchetti

# Phase relations of potassium-bearing clinopyroxene in the system $CaMgSi_2O_6$-$KAlSi_2O_6$ at 7 GPa

Received: 27 February 2003 / Accepted: 3 June 2003 / Published online: 6 August 2003


**Abstract** The pseudo-binary system $CaMgSi_2O_6$-$KAlSi_2O_6$, modeling the potassium-bearing clinopyroxene (*KCpx*) solid solution, has been studied at 7 GPa and 1,100–1,650 °C. The *KCpx* is a liquidus phase of the system up to 60 mol% of $KAlSi_2O_6$. At higher content of $KAlSi_2O_6$ in the system, grossular-rich garnet becomes a liquidus phase. Above 75 mol% of $KAlSi_2O_6$ in the system, *KCpx* is unstable at the solidus as well, and garnet coexists with kalsilite, Si-wadeite and kyanite. No coexistence of *KCpx* with kyanite was observed. Above the solidus, $KAlSi_2O_6$ content of the *KCpx* coexisting with melt increases with decreasing temperature. Near the solidus of the system (about 1,250 °C) *KCpx* contains up to 5.6 wt% of $K_2O$, i.e. about 22–26 mol% of $KAlSi_2O_6$. Such high concentration of potassium in *KCpx* is presumably the maximal content of $KAlSi_2O_6$ in the Fe-free clinopyroxene at 7 GPa. In addition to the major substitution $Mg^{M1}Ca^{M2} \Leftrightarrow Al^{M1}K^{M2}$, the *KCpx* solid solution contains Ca-Eskola and only minor Ca-Tschermack components. Our experimental results indicate that the natural assemblage *KCpx* + grossular-rich garnet might be a product of crystallization of the ultra-potassic $SiO_2$-rich alumino-silicate mantle melts (> 200 km).

O. G. Safonov (✉) · Y. A. Litvin
Institute of Experimental Mineralogy,
Russian Academy of Sciences,
Chernogolovka, 142432 Moscow, Russia
E-mail: oleg@iem.ac.ru
Tel.: +7-096-5246205
Fax: +7-096-5249687

L. L. Perchuk
Department of Geology, Moscow State University,
Vorobievy Gory, 119899 Moscow, Russia

L. Bindi · S. Menchetti
Dipartimento di Scienze della Terra,
University of Firenze, Via La Pira 4, 50121 Firenze, Italy

Editorial responsibility: J. Hoefs

## Introduction

The $K_2O$ content in natural clinopyroxenes rarely exceeds 2 wt% (Ghorbani and Middlemost 2000; Bindi et al. 2003). The majority of potassium-bearing clinopyroxenes (*KCpx*) are described as inclusion in diamonds (Prinz et al. 1975; Moore and Gurney 1985; Rickard et al. 1989; Harlow and Veblen 1991; Harlow 1999) or in eclogitic and peridotitic nodules from kimberlites and lamproites (McGregor and Carter 1970; Reid et al. 1976; Bishop et al. 1978; McCandless and Gurney 1986; Jaques et al. 1990). Inclusions of the *KCpx* in diamonds are often associated with ultra-high pressure phases, such as majoritic Na-bearing garnet and ferropericlase (e.g., Stachel et al. 2000). *KCpx* (with up to 1.5 wt% $K_2O$) coexisting with diamond, coesite, and Al-sphene was also described in garnet-clinopyroxene alumino-silicate and carbonate-silicate rocks of the Kokchetav metamorphic complex, N. Kazakhstan (Sobolev and Shatsky 1990; Perchuk et al. 1995, 1996, 2002; Perchuk and Yapaskurt 1998).

In contrast to the data on natural samples, results of experimental studies of both the model and natural alumino-silicate systems (Shimizu 1971; Edgar and Vukadinovic 1993; Edgar and Mitchell 1997; Mitchell 1995; Luth 1992, 1995, 1997; Tsuruta and Takahashi 1998; Wang and Takahashi 1999; Harlow 1999, 2002), as well as of carbonate-silicate systems at $P > 5$ GPa (Harlow 1997; Matveev et al. 1998; Chudinovskikh et al. 2001) show that about 2 wt% is not a limit for the $K_2O$ content in clinopyroxene. Many authors reported 2.5–3.7 wt% (e.g., Luth 1992; Edgar and Mitchell 1997; Harlow 1999) and up to 5.75 wt% (Chudinovskikh et al. 2001) of $K_2O$ in clinopyroxene from alumino-silicate and carbonate-silicate systems, respectively. A possible reason for the difference in potassium contents in natural *KCpx* and their synthetic analogues is the difference in potassium activity ($a_K^{liq}$) in media (melts, fluids) of their formation. For instance, natural *KCpx* with 1.5% of $K_2O$ are characteristics for the eclogite and peridotite

nodules from kimberlites, as well as for the potassium-poor (~0.2 wt% of $K_2O$) *Grt-Cpx* rocks from the Kokchetav Complex. In turn, most experiments used potassium-rich starting mixtures. For example, Edgar and Vukadinovic (1993), Mitchell (1995), and Edgar and Mitchell (1997) used natural lamproites as starting materials for experiments in carbonate-free systems, while the $K_2O$ content in the lamproite was much higher than that of the common *KCpx*-bearing rocks. Harlow (1997) showed that clinopyroxene with more than 1 wt% of $K_2O$ could crystallize only in equilibrium with carbonate melt containing 14–33 wt% of $K_2O$. Thus, a high potassium activity in a system is one of the major thermodynamic parameters in crystallization of *KCpx* under UHP conditions.

Existing experimental data unambiguously imply that pressure greater than 5 GPa is required for the entering of K into the clinopyroxene structure. The thermodynamic treatment of these data only allows developing of a semi-empirical model and equation for the *KCpx*/melt equilibria (Perchuk et al. 2002). Thermodynamics of potassium jadeite as the end-member and mixing properties of its solid solution with diopside are unknown. For this reason, an application of the *KCpx* equilibria for quantitative estimating the thermodynamic conditions of the formation of UHP rocks is impossible.

This paper presents an experimental study of the system $CaMgSi_2O_6$–$KAlSi_2O_6$ that is the simplest model for the potassium-bearing clinopyroxene solid solution. The specific pressure of 7 GPa has been chosen since it is the highest average pressure for the *Kfs* stability field within a wide temperature range (e.g., Urakawa et al. 1994). *KCpx* has never been observed in natural samples in paragenesis with *Kfs*, whereas the latter mineral is a common product of the *KCpx* decomposition (e.g., Reid et al. 1976; Perchuk et al. 1996, 2002). One purpose of our experiments is the determination of the maximal content of $KAlSi_2O_6$ in diopside at 7 GPa, that limits the *Kfs* stability. Our experimental study of the $CaMgSi_2O_6$-$KAlSi_2O_6$ system seems to be very useful for the derivation of both the phase equilibria diagram and the thermodynamic description of mixing properties of the *Di-KJd* solid solution. The results of our study are also important for a better understanding of the structural modifications in aluminum-bearing potassium-rich clinopyroxenes inferred by the $CaMg \rightarrow KAl$ substitution (Bindi et al. 2002).

## Starting materials, experimental technique, and analytical procedures

The mixtures of stoichiometric gels of $CaMgSi_2O_6$ and $KAlSi_2O_6$ compositions were used as starting materials. The gels were prepared using the nitrate method (Hamilton and Henderson 1968). About 20 mg of a distinct mixture was placed into a Pt ($T < 1{,}500$ °C) or $Pt_{60}Rh_{40}$ ($T > 1{,}500$ °C) capsule. The capsule with charge was subsequently dried for several hours at a temperature of 110 °C and hermetically sealed. Although the starting mixtures were dried before the runs, the presence of some amount of water could not be completely avoided.

The runs were performed at $P = 7$ GPa and $T = 1{,}100$–$1{,}650$ °C with the high-pressure "anvil-with-hole" apparatus (Litvin 1990), which is a modification of the Bridgmen-type anvil assembly (cf. Bradley 1969). Our apparatus is characterized by the homogeneous distribution of pressure and temperature (about 1 °C/mm) in the reaction volume of 0.1–0.15 $cm^3$. The thoroughly designed lithographic stone (marble from the Algeti area, Georgia) was used as a high-pressure cell individually for each run (Fig. 1). The cell is equipped with a graphite heater 7.2 mm in length, 7 mm in diameter, and 0.5 mm wall thickness. The individual capsule was placed in the center of the cell on the special holders made of the pressed MgO and BN mixture (MgO:BN = 3:1). Pressure in the cell was reached by the uni-axial compression of upper and lower anvils by a hydraulic press with a load of 500 t. Pressure at room temperature in the cell was calibrated on the basis of the variations in the resistance of bismuth resulted from the standard phase transitions at 2.55 (Bi I–Bi II), 2.7, and 7.7 (Bi III–Bi V) GPa (Homan 1975). The pressure values at high temperature were also corrected with the diamond-graphite curve (Kennedy and Kennedy 1976). As a result, the run pressure was controlled within the accuracy range ±0.2 GPa. The temperature-current power dependence of the cell was calibrated using a $Pt_{70}Rh_{30}/Pt_{94}Rh_6$ thermocouple. No pressure correction was added to the calibration of the thermocouple. The run temperature was controlled within the accuracy of ±20 °C.

The experiments started with an increase of pressure to the desired values (15–20 min, depending on the target pressure). Subsequently, the charge was heated to the desired temperature in a time period 5–10 min. Depending on temperature, the run duration varied from 30 min to 14 h (Table 1).

Subsequently, each sample was embedded in epoxy and polished for the study of texture and compositions of the products with a microprobe. After preliminary examination in reflected light, the microscopic features of the run products were studied by means of BSE using a CamScan electron microscope. Phase compositions were determined with electron microprobes EDS Link AN10/85S and wave-length Camebax SX50. Microprobe analyses of the phases were performed at 15 kV accelerating potential, 10 nA beam current, and beam diameter of 3 μm. Microprobe analyses of glass (or the products of quenching) were made using a defocused beam or scanning of area 10×10 μm. Natural augite (Si, Al, Mg, Ca) and orthoclase (K) were used as standards. The link analyses were automatically normalized to 100%. No deviations greater than ±2% were observed for the major oxides.

Single-crystal structure refinement of clinopyroxene crystals was reported by Bindi et al. (2002). All attempts to extract crystals of other produced phases for the single-crystal XRD refinement have failed because of small size of the crystals. Some $KAlSi_2O_6$-rich samples were examined by X-ray powder diffraction using CoKα radiation, Fe-filter, and silicon as an internal standard. The hexagonal ($P6_3/m$) $K_2Si_4O_9$ (*SWd*) near the solidus of pure $KAlSi_2O_6$ (see samples 633, 635, Table 1) was identified from the most intense diffraction lines of (112), (201), (103), (111), (121), and (006) (Swanson and Prewitt 1983). Kyanite in the same samples was identified by only two diffraction lines of (200) and (014). The most difficult problem was to identify kalsilite, since some of its diffraction lines are usually overlapped with the diffraction lines of

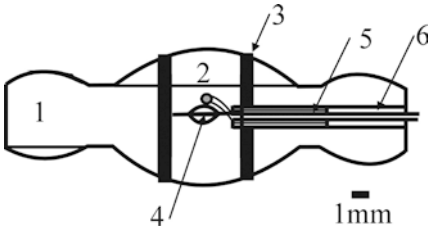


**Fig. 1** A scheme of the cell used in the experiments: *1* cell frame (lithographic stone); *2* sample holder (MgO:BN = 3:1, wt. ratio); *3* heater (graphite); *4* sample in the Pt or $Pt_{60}Rh_{40}$ capsule; *5* thermocouple ($Pt_{70}Rh_{30}/Pt_{94}Rh_6$); *6* insulator

**Table 1** Run conditions and products, produced in the system $CaMgSi_2O_6$–$KAlSi_2O_6$at 7 GPa

| Run no. | $KAlSi_2O_6$ content in the initial mixture (mol%) | Temperature (°C) | Time (min) | Run products[a] |
|---|---|---|---|---|
| 610 | 10 | 1,600 | 120 | *Cpx, $G_S$,Q* |
| 605 | 10 | 1,400 | 180 | *Cpx, $G_S$,Q* |
| 664 | 10 | 1,180 | 315 | *Cpx* |
| 767 | 15 | 1,350 | 180 | *Cpx* [$SiO_2$] |
| 609 | 30 | 1,600 | 120 | *Cpx, $G_S$,Q* [MgO, *Fo*] |
| 661 | 30 | 1,480 | 135 | *Cpx, $G_S$,Q* |
| 604 | 30 | 1,400 | 180 | *Cpx, $G_S$,Q* |
| 653 | 30 | 1,200 | 240 | *Cpx, Grt,SWd* |
| 611 | 50 | 1,600 | 120 | *KCpx, $G_S$,Q* [*Fo*] |
| 780 | 50 | 1,500# | 95 | *KCpx, Grt,$G_S$* |
| 603 | 50 | 1,400 | 180 | *KCpx, $G_S$,Q* [*Fo*, $SiO_2$] |
| 740 | 50 | 1,300 | 240 | *KCpx, Grt,$G_S$, Q* |
| 643 | 50 | 1,200 | 240 | *Cpx, Grt* (?), *SWd* |
| 790 | 60 | 1,550 | 60 | *KCpx***, $G_S$ |
| 781 | 60 | 1,500 | 100 | *KCpx, Grt, SWd*(?), $G_S$ |
| 791 | 60 | 1,400 | 165 | *KCpx, Grt, $G_S$* |
| 688 | 60 | 1,310# | 240 | *KCpx***, *Grt, SWd, $G_S$*(?), *Q* |
| 930 | 60 | 1,300 | 90 | *KCpx, Grt, SWd, Q* |
| 940 | 60 | 1,300 | 180 | *KCpx, Grt, SWd, Q* |
| 869 | 60 | 1,220 | 380 | *KCpx, Grt, SWd, Q* |
| 660 | 70 | 1,500 | 120 | *Grt, $G_S$* |
| 650 | 70 | 1,350 | 180 | *KCpx***, *Grt, Q* |
| 665 | 70 | 1,200 | 330 | Cpx, Grt, SWd, Q |
| 671 | 70 | 1,100 | 805 | *Cpx, Grt, SWd* |
| 808 | 75 | 1,470 | 110 | *Grt, $G_S$* |
| 805 | 75 | 1,360 | 210 | *Grt**, *SWd* (?), *$G_S$, Q* |
| 816 | 75 | 1,300 | 240 | *Grt, SWd, $G_S$* (?), *Q* |
| 833 | 80 | 1470 | 110 | *Grt, $G_S$* |
| 807 | 80 | 1,370 | 210 | *Grt**, *$G_S$* |
| 817 | 80 | 1,320 | 240 | *Grt**, *SWd* (?),*$G_S$* (?), *Q* |
| 686 | 85 | 1,460 | 125 | *Grt, $G_S$* |
| 687 | 85 | 1,360 | 180 | *Grt, $G_S$,Q* |
| 683 | 85 | 1,290 | 270 | Grt, SWd, Ky, Q |
| 855 | 90 | 1,350 | 145 | *$G_S$* [$Al_2O_3$] |
| 856 | 90 | 1,300 | 180 | *Grt**, *$G_S$* |
| 870 | 90 | 1,200 | 215 | *Grt, SWd, Ky* (?), *Q* |
| 634 | 100 | 1,650 | 30 | *Ks, $G_S$,Q* |
| 633 | 100 | 1,400 | 60 | *SWd**, *Ky**, *Ks, $G_S$* |
| 676 | 100 | 1,300 | 240 | *SWd, Ks* (?), *Ky* (?) |
| 635 | 100 | 1,200 | 90 | *SWd**, *Ks,Ky** |

[a](?) Phase is not surely identified; *Q* products of quenching of the alumino-silicate glass (see text); *[.]* rare, metastable phases; * presence of the phase is confirmed by the powder XRD analysis; ** phase is studied by the single-crystal XRD analysis (Bindi et al. 2002and unpublished data); # the starting run temperature; the final run temperature was lower by about 50 °C

*SWd*. However, an existence of several diffraction lines, e.g., (004), (105), probably correspond to the hexagonal polymorph of $K_8Al_8Si_8O_{32}$ rather than the orthorhombic one.

Table 1 shows both the run conditions and products. Figure 2a–f illustrates textural relations in some experimental samples. In most cases, the experimental samples show fine-grained textures with prevailing grain size of about 10–20 μm. The texture of the samples and the degree of crystallization of the phases depended on the temperature of each individual run and its duration. The most spectacular textures with highly idiomorphic clinopyroxene crystals of up to 100 μm in size were obtained in runs with $KAlSi_2O_6$-rich charges at 1,200–1,350 °C and run durations of 180–380 min (Fig. 2c–e). In the case of the $KAlSi_2O_6$-poor charges, the *Cpx* forms subhedral grains of different sizes and it is often intergrown with cloudy *SWd* (Fig. 2a). Garnet in the run products forms euhedral rounded crystals uniformly distributed within the separate samples (Fig. 2b–f). In some cases, garnet grains are included into larger clinopyroxene grains or located at their boundaries. Granular textures are observed in the samples that are pure in $KAlSi_2O_6$. Kyanite in the $KAlSi_2O_6$-pure samples forms rare tiny crystals, intergrown with Si-wadeite or as inclusions in kalsilite.

In most cases, the presence of former alumino-silicate melt is identified by spectacular quenched textures (e.g., Fig. 2a, d, e). These textures are characterized by fibrous or interlaced aggregates of various phases (see below). In most samples (Table 1), they are mica-like phases (see below), which locally form large flakes in the matrix (see Fig. 2e). The flakes contain numerous inclusions of small garnet grains as well as surround large *KCpx* grains. It is evident that the flakes were formed after formation of garnet and *KCpx* during quenching of the alumino-silicate melt. Along with quenching textures, separate areas of pure glass ($G_s$) are observed. In *Di*-poor (mostly without *Cpx*) portion of the system, the alumino-silicate glass is more homogeneous (Fig. 2f), but locally shows diverse quenched textures as well. The detection of the alumino-silicate glass near the solidus is very inadequate. For example, sample 767 (Table 1) consists of large anhedral grains of clinopyroxene, forming solid matrix. In turn, sample 605 (Table 1) contains localized areas composed of the mica-like phases between large anhedral clinopyroxenes grains. It is very difficult to discern, whether these localized areas are remnants of quenched melt or remnants of the under-reacted material, preserved within the clinopyroxene matrix. Similar problem arises in the $KAlSi_2O_6$-rich portions of the system as well.

Some samples (as a rule, high temperature runs) contain rare metastable phases (see Table 1). Most of them show reaction relationships with major phases. For example, periclase, MgO, in sample 609 (Table 1) forms aggregate rimmed by forsterite at the contacts with clinopyroxene crystals. Forsterite and $SiO_2$ form rare tiny grains associated with the quenching textures or included in large clinopyroxene crystals. Rare grains of $SiO_2$ are detected in the

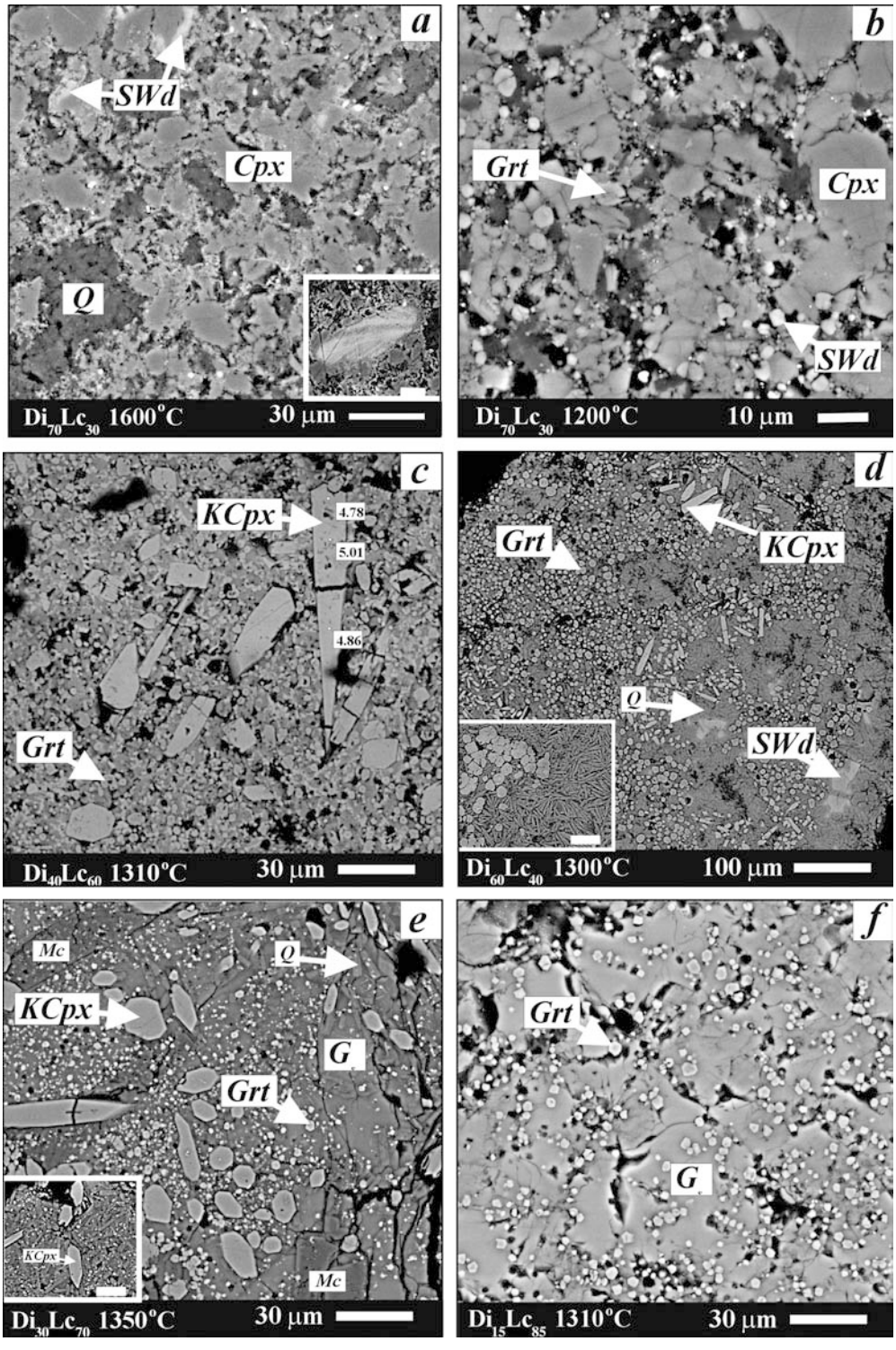


**Fig. 2a–f** BSE images of textural phase relationships in some run products in the system $CaMgSi_2O_6$–$KAlSi_2O_6$ at 7 GPa. **a** Separate anhedral *Cpx* crystals intergrown with cloudy *SWd* (*white spots* in clinopyroxene) with quench products (*Q*) of the alumino-silicate glass in the run 609 (Table 1); the detail view of the *SWd* "cloud" in *Cpx* is shown in the *inset* (scale 10 μm); **b** Assemblage *Grt* + *Cpx* + *SWd* in the subsolidus of the system (run 653; Table 1); **c** elongated idiomorphic crystals of ultra-potassic *KCpx* coexisting with *Grt* near the solidus of the system (run 688; Table 1); light-gray matrix in the interstices is composed of quench products of the remnant alumino-silicate glass; figures in the *KCpx* field indicate $K_2O$ content (wt%); **d** separate idiomorphic crystals of ultra-potassic *KCpx* (up to 4.5 wt% of $K_2O$) coexisting with abundant rounded *Grt* and large *SWd* anhedral grains in the matrix of quenched alumino-silicate glass (run 930; Table 1); the inset shows the detail view of rounded garnets plunged into the spectacular quenched textures (scale 30 μm); **e** idiomorphic crystals of *KCpx* coexisting with *Grt* and *SWd* (*small white grains*) in the matrix, that locally consists of fibrous or elongated crystals of quenched phases (*Q*) and large flakes of mica-like phase (*Mc*) along with relatively clear glass ($G_s$); the detail view of the quenched textures is shown in the *inset* (scale 30 μm; run 650; Table 1). **f** Small idiomorphic *Grt* crystals in homogeneous alumino-silicate glass (run 686; Table 1)

solidus of the *Di*-rich portion of the system as well. Corundum ($Al_2O_3$) in sample 855 (Table 1) forms needle-like crystals, formed during quenching of the alumino-silicate glass.

## The topological analysis and T–X diagram for the pseudo-binary system $CaMgSi_2O_6$–$KAlSi_2O_6$

Bowen and Schairer (1929) showed that the system diopside-leucite at 1 atm is characterized by simple eutectic relationships. No potassium solubility in diopside was observed. At a pressure of 11 GPa, Luth (1992) synthesized clinopyroxene with 3 wt% of $K_2O$ in the diopside-leucite mixtures. However, no systematic experimental data on the system $CaMgSi_2O_6$–$KAlSi_2O_6$ at high pressures exist. At $P > 3$ GPa leucite breaks down to produce the assemblage *Ks* + *SWd* + *Ky* (Liu 1987; Fasshauer et al. 1998). As a result, the simple binary

system diopside-leucite at ambient pressure transforms into the complicated pseudo-binary system at 7 GPa.

The T–X phase diagram for the complex pseudo-binary system can be constructed only on the basis of original experimental data along with the detailed topological analysis of the system (Maaløe 1985). An approach involving the combination of the topological analysis and original experimental data was successfully applied in study of melting relations in some complex Na-bearing systems involving UHP *Cpx* (Gasparik and Litvin 1997). The approach includes the following procedures: (i) evaluation of possible sub-solidus phase assemblages; (ii) evaluation of possible liquidus surfaces, cotectic lines, and eutectic points; (iii) construction of a schematic phase diagram using the Rhines' theorem (Rhines 1956; Maaløe 1985); (iv) specification of phase fields in the T–X grid using the available experimental data. It is impossible to model a complex pseudo-binary system only on the basis of experimental data without the above procedures.

## Choice of components

We tentatively regarded that the Ca/Mg ratio in garnet and clinopyroxene is constant, while *KCpx* is the only potassium-bearing solid solution. Other phases were suggested to be of constant potassium content. These simplifications allow transformation of the five-component system $K_2O$–CaO–MgO–$Al_2O_3$–$SiO_2$ into a quaternary $K_2O$–(Ca, Mg)O–$Al_2O_3$–$SiO_2$ by combination of CaO and MgO into one component. Figure 3a, b presents the topology of the pseudo-binary system $CaMgSi_2O_6$–$KAlSi_2O_6$ in terms of the quaternary system $K_2O$–(Ca, Mg)O–$Al_2O_3$–$SiO_2$.

## Evaluation of possible sub-solidus phase fields

The subsolidus of the system at 7 GPa involves *KCpx*, *Grt*, *SWd*, *Ks*, and *Ky* (Table 1). Three latter phases are the products of $KAlSi_2O_6$ decomposition (Liu 1987; Fasshauer et al. 1998) due to reaction:

$$3''Lc'' = Ks + SWd + Ky. \quad (1)$$

The *KCpx* and the *Grt* solid solutions are the products of the reactions between starting *Di* and "*Lc*" = *SWd* + *Ks* + *Ky*, e.g.,

$$3Di + 4/3Ks + 4/3Ky = Prp + Grs + 2/3SWd \quad (2)$$

$$3Di + 2Ks + 2Ky = 2KJd + Prp + Grs \quad (3)$$

Among numerous complex equilibria in the system, the following ones demonstrate that both the Ca-*Ts* and Ca-*Esk* components in *KCpx* are also the products of reaction of starting *Di* with *SWd, Ks,* and *Ky*:

$$3Di + 4Ky = Prp + 8/3\mathrm{Ca} - Esk + 5/3Ca - Ts \quad (4)$$

$$3Di + 8/3Ks + 8/3Ky = 3\mathrm{Ca} - Ts + Prp + 4/3SWd \quad (5)$$

$$3Di + 5/3SWd + 17/3Ky = 6\mathrm{Ca} - Esk + Prp + 10/3Ks \quad (6)$$

Thus, compositions of all phases in the system are outside the binary join *Di*-"*Lc*". This is the general determining feature of any pseudo-binary system (Rhines 1956; Maaløe 1985).

The position of *Di*, *Grt*, *SWd*, *Ks*, and *Ky,* within the $K_2O$-(Ca, Mg)O-$Al_2O_3$-$SiO_2$ tetrahedron is shown in the inset picture of Fig. 3a. The stable assemblage *Grt* + *SWd* (Table 1) in the subsolidus of the system suggests corresponding tie-line in Fig. 3a. As a result, the above major five end-member phases compose three distorted tetrahedrons: *Di-Ky-SWd-Grt*, *Di-Ks-SWd-Grt*, and *Grt-Ks-Ky-SWd*. The join *Di*-"*Lc*" is coplanar with the plane *Di-SWd-Grt* (gray plane in Fig. 3a) that separates the tetrahedron *Di-Ky-SWd-Grt* from the tetrahedron *Di-Ks-SWd-Grt*. It intersects the tie-line *Grt* + *SWd* and penetrates the tetrahedron *Grt-Ks-Ky-SWd*. Since the join is involved in the plane *Di-SWd-Grt* and the tetrahedron *Grt-Ks-Ky-SWd* only, Fig. 3a shows these geometric elements and omits other adjacent tetrahedrons.

Potassium-bearing clinopyroxene is the complex solid solution of at least four end members, *Di*, *KJd*, Ca-*Esk*, Ca-*Ts* (see below). These components form a small tetrahedron $KCpx_{ss}$ in Fig. 3a. The *Di*, Ca-*Ts* and *KJd* apexes are situated on the *Di-SWd-Grt* plane, while Ca-*Esk* apex is below this plane. An appearance of $KCpx_{ss}$ results in three additional tetrahedrons, i.e. $KCpx_{ss}$-*Grt,* $KCpx_{ss}$-*SWd*, and $KCpx_{ss}$-*Grt-SWd* (Fig. 3a). The formation of the $KCpx_{ss}$ also results in slight displacement of the starting point of true join $KCpx_{ss}$-"*Lc*" away from the *Di–SWd–Grt* plane inwards the $KCpx_{ss}$ tetrahedron. Starting in some point inside the $KCpx_{ss}$ tetrahedron, the join (see thick dashed line in Fig. 3a) goes through the $KCpx_{ss}$, $KCpx_{ss}$-*Grt* and $KCpx_{ss}$-*SWd-Grt* tetrahedrons. Subsequently, the join crosses the boundary *Grt-SWd*, indicating the reaction:

$$3Di(\mathrm{in}KCpx) + 4''Lc'' = Prp + Grs + 2SWd \quad (7)$$

and penetrates the tetrahedron *Grt-Ks-Ky-SWd*. The end of the join lies in the center of the *Ky-SWd-Ks* plane, indicating the reaction (1). Such position of the join $KCpx_{ss}$-"*Lc*" outlines four major sub-solidus phase assemblages at a given bulk composition along the join: $KCpx_{ss}$, $KCpx_{ss}$ + *Grt*, $KCpx_{ss}$ + *Grt* + *SWd*, and *Grt* + *Ks* + *SWd* + *Ky*.

## Evaluation of possible liquidus, cotectics and eutectics

Figure 3b shows schematically possible liquidus surfaces, cotectic lines and eutectic points within the $KCpx_{ss}$-*Grt-SWd* and the *Grt-Ks-Ky-SWd* volumes. Using this construction, we can determine the possible

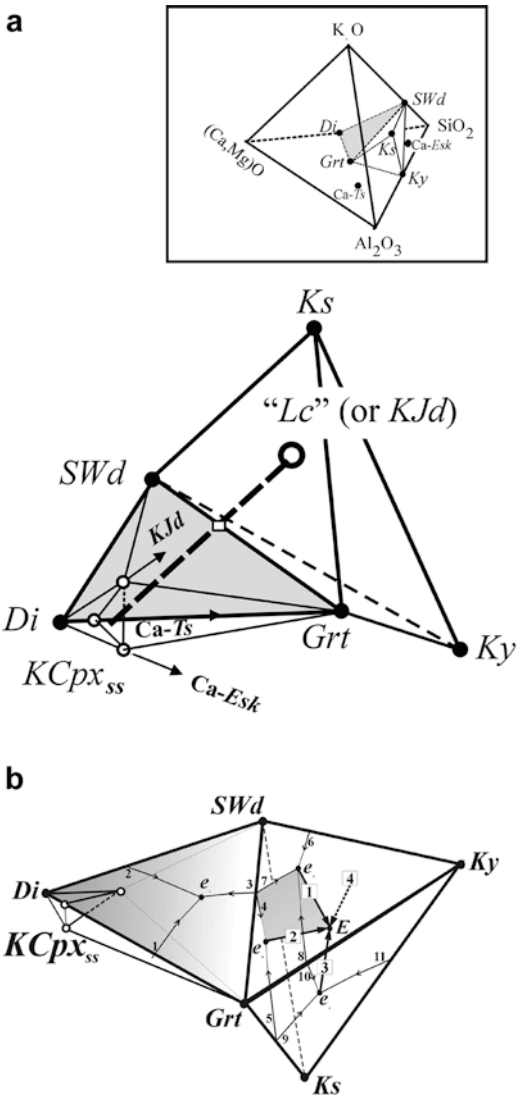


**Fig. 3** The topological analysis of the pseudo-binary system $CaMgSi_2O_6$–$KAlSi_2O_6$ at 7 GPa. **a** The relative position of phases and the studied join within the tetrahedron $K_2O$-(Ca, Mg)O–$Al_2O_3$–$SiO_2$. Both in the *main picture* and the *inset*, *solid lines* indicate the visible lines, whereas *dashed lines* show the invisible lines. *Inset* Position of phases (*Grt, SWd, Ks, Ky*) and components of the *Cpx* solid solution (*Di*, Ca-*Ts*, Ca-*Esk*) within the tetrahedron $K_2O$-(Ca, Mg)O-$Al_2O_3$-$SiO_2$ (*black dots*). The *Di-SWd-Grt* plane is *shaded*. Tie-lines *Di-Ky* and *Di-Ks* are not shown in favor of better view. *Main picture* The detailed view of the *Di-SWd-Grt* plane (*shaded*), the *Grt-Ks-SWd-Ky* tetrahedron and the $KCpx_{ss}$-"*Lc*" join (*bold dashed line*). *Empty rectangle* indicates a crossing of the *Grt-SWd* boundary by the join $KCpx_{ss}$-"*Lc*". *Empty dots* indicate a displacement of the $KCpx_{ss}$ composition owing to the *KJd*, Ca-*Ts* and Ca-*Esk* substitutions (directions are shown by *arrows*). *Thinner lines* indicate the $KCpx_{ss}$ tetrahedron and its connections with the *Grt* apex (the connection with the *SWd* apex is not shown). The actual relative position of phases is distorted in favor of better view. See text for further explanations. **b** A schematic position of eutectics and cotectic lines within the $KCpx_{ss}$-*SWd-Grt* and the *Grt-Ks-SWd-Ky* tetrahedrons. Eutectics: $e_1$ $KCpx_{ss}+Grt+SWd+L$; $e_2$ $Grt+SWd+Ky+L$; $e_3$ $Grt+Ks+SWd+L$; $e_4$ $Grt+Ks+Ky+L$; *E* $Grt+SWd+Ks+Ky+L$; eutectic $Ks+SWd+Ky+L$ within the $Ks+SWd+Ky$ plane is not shown. Ternary cotectic lines: *1* $KCpx_{ss}+Grt+L$; *2* $KCpx_{ss}+SWd+L$; *3*, *4*, *7* $Grt+SWd+L$; *5*, *9* $Grt+Ks+L$; *6* $SWd+Ky+L$; *8*, *10* $Grt+Ky+L$. Quaternary cotectic lines (*boxed figures*): *1* $Grt+SWd+Ky+L$; *2* $Grt+Ks+SWd+L$; *3* $Grt+Ks+Ky+L$; *4* $Ks+SWd+Ky+L$. Ternary cotectic lines within the $Ks+SWd+Ky$ plane are not shown. *Open circles* show a displacement of the $KCpx_{ss}$ composition owing to *KJd*, Ca-*Ts* and Ca-*Esk* substitutions

sequence of phase assemblages, appearing in different portions of the system as temperature drops. The join $KCpx_{ss}$-"*Lc*" involves four-phase eutectic $KCpx_{ss}+Grt+SWd+L$ ($e_1$ in figure 3b) and five-phase eutectic $Grt+Ks+SWd+Ky+L$ (*E* in Fig. 3b). Thus, the crystallization of all melts with composition at the left side from the $Grt+SWd$ boundary stops at the first eutectic. All "*Lc*"-rich melts (>75 mol% of $KAlSi_2O_6$) crystallize at the second eutectic. The specific melt, containing about 75 mol% $KAlSi_2O_6$, crystallizes into binary assemblage $Grt+SWd$. We suggest that this is the thermal divide (singular equilibrium field), similar to the $Fo+Cpx$ assemblage in the system enstatite-nepheline at 13 GPa (Gasparik and Litvin 1997).

## Construction of a preliminary phase diagram

The phase diagram for the complex pseudo-binary system can be constructed on the basis of the theorem of general validity stated by Rhines (1956): A field of the phase diagram, representing equilibrium among a given number *N* of phases, can be bounded only by regions representing equilibria among one more or one less ($N\pm1$), than given number of phases *N*; a univariant equilibrium curve should be considered a region (the theorem is quoted from Maaløe 1985, p. 75). Taking into account the above topological analysis (Fig. 3a, b) we constrain the isobaric *T-X* phase diagram using the Rhines' theorem for pseudo-binary systems and original experimental data from Table 1. The diagram in Fig. 4 is characterized by the following general features:

1. *KCpx* solid solution is the only liquidus phase at the $KAlSi_2O_6$-content below ~60 mol% and it is stable up to 75 mol% of $KAlSi_2O_6$ in the solidus.
2. Grossular-rich *Grt* is the liquidus phase at the bulk $KAlSi_2O_6$ content 60–95 mol% and it replaces *KCpx* in the solidus at above 75 mol% of $KAlSi_2O_6$. Garnet, probably, gives place to *Ks* at liquidus, near the pure $KAlSi_2O_6$.
3. High solubility of the *KJd* in clinopyroxene is observed in the system. Above the solidus, the *KJd* content in *KCpx* increases with decreasing temperature (see discussion below), reaching at solidus (~1,250 °C) 22–26 mol% (5.0–5.6 wt% of $K_2O$). The *KJd* content in *KCpx* presumably decreases with decreasing temperature below the solidus.
4. A stable assemblage *KCpx* + grossular-rich *Grt* is synthesized below the liquidus.
5. No peritectic relations are induced both from the topological analysis and the examination of the run products. An absence of peritectic relations in the

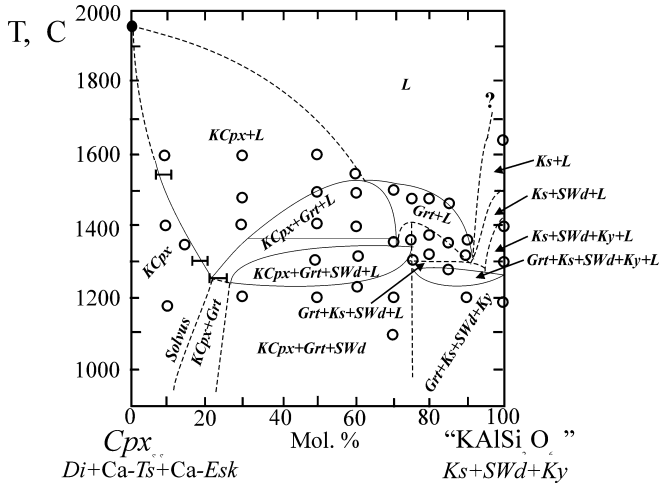


**Fig. 4** Preliminary phase diagram for the pseudo-binary system $CaMgSi_2O_6$–$KAlSi_2O_6$ at 7 GPa constructed on the basis of the topological analysis (see Fig. 3 a, b), the Rhines' theorem, and experimental data in Table 1 (*dots*). *Solid lines* denote experimentally constrained phase boundaries. *Dashed lines* show the phase boundaries, which are not experimentally constrained. *Bars* indicate ranges of *KCpx* composition, taken into account to draw the solidus line (see text). Melting temperature of diopside at 7 GPa, 1,962 °C (*filled circle*) is calculated from data by Gasparik (1996). For the pure composition $KAlSi_2O_6 = Ks + SWd + Ky$ in the subsolidus (e.g., Liu 1987)

system is supported by the compositions of glasses produced in the runs (see below).

6. The thermal divide (singular equilibrium field) $Grt + SWd$ separates two portions of the system.
7. *KCpx* never coexists with *Ky*.
8. The system is characterized by four-phase eutectic $KCpx_{ss} + Grt + SWd + L$ and five-phase eutectic $Grt + Ks + SWd + Ky + L$. The temperatures of the eutectics need more precise determination because of inadequate glass identification. However, we assume that temperature of the $Grt + Ks + SWd + Ky + L$ eutectic is somewhat lower than that of the $KCpx_{ss} + Grt + SWd + L$ eutectic (Fig. 4).

The whole diagram (Fig. 4) has to be considered as tentative, since (1) its $KAlSi_2O_6$-rich portion is not well experimentally constrained and demands further experiments; (2) no other K-bearing solid solutions rather than *KCpx* are considered; (3) no variation of Ca-content of *Grt* is regarded, and (4) no variations of Ca-*Esk* and Ca-*Ts* components is shown in the preliminary two-dimensional diagram. Experimental data allowed us to confirm the general topology of the system and to specify major phase fields, suggested on the basis of the topological analysis.

## Phase compositions

The phases synthesized in the system $CaMgSi_2O_6$–$KAlSi_2O_6$ at 7 GPa show wide compositional variations. Identification of the phases is based on microprobe analyses mostly, since a single-crystal XRD study of most run products is very difficult because of the grain size problem. A structure refinement was performed on clinopyroxene crystals only (Bindi et al. 2002 and unpublished data).

*Clinopyroxene* Wide compositional variations of clinopyroxene (Tables 2, 3, 4) are determined by diffusion effects as well as equilibrium variations of temperature at constant pressure. The following features were chosen as indicators of equilibrium composition of clinopyroxene in each individual run:

1. Compositional homogeneity of clinopyroxene crystals. Euhedral clinopyroxene crystals of up to 100 μm in size (Fig. 2 c–e) allow measuring of their compositional zoning. Relatively unzoned crystals were considered as equilibrium phases.
2. Compositional statistics. The most uniform compositions (within the analytical error) indicate equilibrium.

The compositional homogeneity of clinopyroxene crystals depends on run duration. In order to demonstrate this rule, runs of different duration at the same temperature were carried out. For example, short-term run 930 (Table 1) resulted in crystallization of clinopyroxenes with $K_2O$ content varying from 2.7 to 4.2 wt%, whereas compositional variations of *KCpx* in the long-term run 940 (Table 1) is just 4.1–4.5 wt%. In further modeling, only long-term run data will be regarded.

At $< 50$ mol% of $KAlSi_2O_6$ in the system, *Cpx* in the run products contains less than 0.4 wt% of $K_2O$ (see Tables 2, 3, 4). Clinopyroxene crystals in these run products are significantly heterogeneous in their composition, exhibiting locally a predominance of K over Al and an excess of Si in the formula of mineral (see empty rectangles in Fig. 5a). These features are resulted from contamination with micron-size inclusions of Si-wadeite. This suggestion is supported by the presence of the cloudy intergrowth of clinopyroxene and Si-wadeite (Fig. 2a). The Al/K ratio in clinopyroxene directly depends on the $KAlSi_2O_6$ content in the initial mixture: the larger the $KAlSi_2O_6$ content the closer this ratio is to 1. All these features imply that in a case of the $KAlSi_2O_6$-poor mixtures, diffusion is the only reason for compositional heterogeneity of clinopyroxene and the absence of relatively high potassium content in it.

Clinopyroxene crystals containing 1–5.62 wt% of $K_2O$ were identified in the runs with 50–70 mol% of $KAlSi_2O_6$ only (Fig. 2c–e). Near the liquidus, the $K_2O$ content in cores of *KCpx* grains reaches 2.5–3.2 wt% (Tables 2, 3, 4). These clinopyroxenes grains are saturated in $Al_2O_3$ as well. The highest concentration of $Al_2O_3$ (up to 11.9 wt%) is observed in clinopyroxenes in the *Grt*-absent assemblage synthesized at higher temperature (e.g., run 790, Tables 1, 2, 3, 4). As a rule, crystals of potassium-bearing clinopyroxenes synthesized in high-temperature runs are inhomogeneous in composition, probably because of the short time of the

**Table 2** Representative individual point analyses (runs 610, 653, 611, 780) of phases produced in some experiments in the system $CaMgSi_2O_6$-$KAlSi_2O_6$ at 7 GPa

| Run no. | 610 | | | | 653 | | | 611 | | | | 780 | | | |
|---|---|---|---|---|---|---|---|---|---|---|---|---|---|---|---|
| Phase | *Cpx*[a] | *Cpx*[b] | *SWd*[c] | $G_S$ | *SWd* | *Cpx* | *Grt* | *Cpx* | *KCpx* | *KCpx* | $G_S$ | *KCpx* | *KCpx* | *Grt* | $G_S$ |
| $SiO_2$ | 56.23 | 57.22 | 72.76 | 61.45 | 73.35 | 55.78 | 42.18 | 55.92 | 55.67 | 56.01 | 60.67 | 55.67 | 55.26 | 42.00 | 60.58 |
| $Al_2O_3$ | 0.02 | 0.01 | 0.16 | 16.12 | 0.21 | 0.34 | 23.07 | 0.09 | 3.39 | 1.04 | 12.91 | 4.25 | 5.02 | 22.69 | 19.22 |
| MgO | 19.04 | 19.08 | 0.24 | 8.87 | 0.02 | 18.82 | 10.77 | 18.56 | 15.69 | 18.46 | 13.30 | 15.27 | 14.65 | 10.38 | 4.62 |
| CaO | 25.04 | 24.74 | 0.28 | 0.21 | 0.13 | 24.47 | 23.03 | 25.18 | 22.02 | 23.74 | 1.68 | 21.12 | 20.76 | 24.39 | 1.46 |
| $K_2O$ | 0.22 | 0.14 | 26.55 | 13.35 | 26.05 | 0.35 | 0.30 | 0.21 | 2.53 | 1.05 | 11.44 | 3.70 | 4.29 | 0.53 | 14.12 |
| Total | 100.55 | 101.18 | 99.99 | 99.99 | 99.76 | 99.76 | 99.36 | 99.96 | 99.29 | 100.31 | 100.00 | 100.01 | 99.98 | 99.99 | 100.00 |
| Formula ratio per given O | | | | | | | | | | | | | | | |
| O | 6 | 6 | 9 | 24 | 9 | 6 | 12 | 6 | 6 | 6 | 24 | 6 | 6 | 12 | 24 |
| Si | 2.010 | 2.026 | 4.008 | 8.508 | 4.023 | 2.006 | 3.041 | 2.012 | 2.013 | 2.006 | 8.414 | 2.005 | 1.995 | 3.036 | 8.425 |
| Al | 0.001 | 0.001 | 0.010 | 2.630 | 0.013 | 0.015 | 1.960 | 0.004 | 0.144 | 0.044 | 2.110 | 0.180 | 0.214 | 1.932 | 3.149 |
| Mg | 1.014 | 1.006 | 0.020 | 1.829 | 0.002 | 1.008 | 1.157 | 0.995 | 0.845 | 0.985 | 2.748 | 0.819 | 0.788 | 1.118 | 0.957 |
| Ca | 0.959 | 0.938 | 0.017 | 0.031 | 0.008 | 0.942 | 1.778 | 0.970 | 0.853 | 0.911 | 0.249 | 0.815 | 0.802 | 1.888 | 0.218 |
| K | 0.010 | 0.006 | 1.865 | 2.358 | 1.822 | 0.016 | 0.028 | 0.009 | 0.117 | 0.048 | 2.024 | 0.170 | 0.197 | 0.049 | 2.504 |
| Total | 3.994 | 3.977 | 5.919 | 15.355 | 5.868 | 3.987 | 7.965 | 3.990 | 3.972 | 3.994 | 15.544 | 3.989 | 3.996 | 8.023 | 15.253 |
| $Al^{IV}$ | 0.000 | 0.000 | | | | 0.000 | | 0.000 | 0.000 | 0.000 | | 0.000 | 0.005 | | |
| $Al^{VI}$ | 0.001 | 0.001 | | | | 0.015 | | 0.004 | 0.144 | 0.044 | | 0.180 | 0.209 | | |
| $Mg^{M1}$ | 0.999 | 0.999 | | | | 0.985 | | 0.996 | 0.856 | 0.956 | | 0.819 | 0.788 | | |
| $Mg^{M2}$ | 0.015 | 0.007 | | | | 0.023 | | 0.000 | 0.000 | 0.029 | | 0.000 | 0.000 | | |
| $X_{Ca}^{Grt(c)}$ | | | | | | | 0.606 | | | | | | | 0.628 | |

[a]Probably contaminated with *SWd*
[b]Cloudy*SWd* in clinopyroxene
[c]$X_{Ca}^{Grt} = Ca/(Ca + Mg)$

**Table 3** Representative individual point analyses (runs 790, 688, 869, 650) of phases produced in some experiments in the system $CaMgSi_2O_6$-$KAlSi_2O_6$ at 7 GPa

| Run no. | 790 | | | 688 | | | | 869 | | | | | 650 | | |
|---|---|---|---|---|---|---|---|---|---|---|---|---|---|---|---|
| Phase | *KCpx* | *KCpx* | *Q*[a] | *KCpx* | *KCpx* | *SWd* | Grt | *KCpx* | *KCpx* | *Grt* | *SWd* | *Q* | *Grt* | *KCpx* | Q |
| $SiO_2$ | 50.93 | 50.87 | 66.20 | 54.89 | 54.71 | 73.53 | 42.88 | 55.35 | 54.73 | 43.19 | 71.10 | 56.07 | 42.03 | 54.15 | 64.31 |
| $Al_2O_3$ | 11.85 | 10.95 | 20.74 | 7.54 | 7.29 | 0.51 | 23.62 | 7.12 | 6.57 | 23.60 | 1.04 | 17.74 | 23.52 | 4.90 | 17.06 |
| MgO | 11.89 | 12.20 | 0.08 | 13.36 | 13.30 | 0.00 | 17.04 | 13.13 | 13.95 | 16.79 | 0.58 | 6.29 | 11.20 | 16.50 | 0.28 |
| CaO | 23.80 | 22.74 | 0.04 | 19.30 | 19.24 | 0.00 | 15.42 | 18.78 | 20.18 | 15.79 | 1.69 | 0.00 | 23.09 | 22.71 | 0.68 |
| $K_2O$ | 1.52 | 3.22 | 12.95 | 4.96 | 5.46 | 27.17 | 1.04 | 5.62 | 4.58 | 0.62 | 29.01 | 13.95 | 0.10 | 1.42 | 17.20 |
| Total | 99.99 | 99.98 | 100.01 | 100.00 | 100.00 | 101.22 | 100.00 | 100.00 | 100.01 | 99.99 | 103.43 | 94.05 | 99.93 | 99.67 | 99.53 |
| Formula ratio per given O | | | | | | | | | | | | | | | |
| *O* | 6 | 6 | 8 | 6 | 6 | 9 | 12 | 6 | 6 | 12 | 9 | 11 | 12 | 6 | 8 |
| Si | 1.830 | 1.842 | 2.984 | 1.975 | 1.975 | 4.003 | 3.026 | 1.994 | 1.974 | 3.041 | 3.873 | 3.813 | 3.017 | 1.945 | 3.005 |
| Al | 0.502 | 0.467 | 1.101 | 0.319 | 0.310 | 0.033 | 1.964 | 0.302 | 0.279 | 1.958 | 0.067 | 1.422 | 1.989 | 0.207 | 0.939 |
| Mg | 0.637 | 0.658 | 0.006 | 0.716 | 0.715 | 0.000 | 1.791 | 0.705 | 0.749 | 1.761 | 0.047 | 0.637 | 1.197 | 0.883 | 0.019 |
| Ca | 0.916 | 0.882 | 0.002 | 0.746 | 0.744 | 0.000 | 1.165 | 0.725 | 0.779 | 1.191 | 0.098 | 0.000 | 1.775 | 0.873 | 0.033 |
| K | 0.070 | 0.149 | 0.744 | 0.225 | 0.251 | 1.887 | 0.094 | 0.258 | 0.211 | 0.056 | 2.016 | 1.210 | 0.009 | 0.065 | 1.024 |
| Total | 3.955 | 3.998 | 4.837 | 3.978 | 3.995 | 5.923 | 8.040 | 3.984 | 3.992 | 8.007 | 6.101 | 7.081 | 7.987 | 3.973 | 5.020 |
| $Al^{IV}$ | 0.170 | 0.158 | | 0.025 | 0.025 | | | 0.006 | 0.026 | | | | | 0.055 | |
| $Al^{VI}$ | 0.332 | 0.309 | | 0.294 | 0.285 | | | 0.296 | 0.253 | | | | | 0.152 | |
| $Mg^{M1}$ | 0.637 | 0.658 | | 0.706 | 0.714 | | | 0.704 | 0.747 | | | | | 0.848 | |
| $Mg^{M2}$ | 0.000 | 0.000 | | 0.010 | 0.003 | | | 0.001 | 0.002 | | | | | 0.035 | |
| $X_{Ca}^{Grt(b)}$ | | | | | | | 0.394 | | | 0.403 | | | 0.597 | | |

[a]*Q* denotes phases formed by quenching of the alumino-silicate glass
[b]$X_{Ca}^{Grt} = Ca/(Ca + Mg)$

runs. Cores of larger crystals show the highest concentrations of $K_2O$ and $Al_2O_3$, while they decrease toward rims. As usual, the composition of the rims of larger crystals is close to the composition of smaller crystals. For example, the maximal $K_2O$ concentration (3.2 wt%) of aluminum-rich clinopyroxene from the run 790 (Tables 1, 2, 3, 4) is identified in the core of a large idiomorphic crystal. Smaller crystals in this run and rims of large crystals show distinctly lower, but relatively uniform, $K_2O$ content (1.5–1.8 wt% at similar $Al_2O_3$ content), which is taken to be the equilibrium.

**Table 4** Representative individual point analyses (runs 808, 686, 683, 870, 635) of phases produced in some experiments in the system $CaMgSi_2O_6$–$KAlSi_2O_6$ at 7 GPa

| Run no. | 808 | | 686 | | | | 683 | | | | 870[a] | | | 635 | | | |
|---|---|---|---|---|---|---|---|---|---|---|---|---|---|---|---|---|---|
| Phase | *Grt* | $G_S$ | *Grt* | *Grt* | $G_S$ | $G_S$ | *Grt* | *SWd* | *Ky*[b] | *Q*[c] | *SWd* | *Q* | *Q* | *Ks* | *SWd* | *Ky*[b] | $G_S$ |
| $SiO_2$ | 42.88 | 60.49 | 42.36 | 42.81 | 61.53 | 59.11 | 42.25 | 72.33 | 37.83 | 52.73 | 71.08 | 52.58 | 52.16 | 42.50 | 72.52 | 39.64 | 66.53 |
| $Al_2O_3$ | 23.59 | 18.12 | 23.26 | 23.74 | 21.27 | 19.39 | 23.18 | 0.73 | 61.15 | 25.96 | 0.84 | 25.27 | 26.07 | 43.86 | 1.42 | 58.84 | 11.11 |
| MgO | 13.21 | 0.95 | 14.78 | 16.28 | 1.97 | 1.53 | 11.85 | 0.01 | 0.42 | 5.42 | 0.38 | 5.82 | 5.28 | 0.00 | 0.00 | 0.00 | 0.00 |
| CaO | 19.69 | 0.53 | 19.15 | 16.55 | 0.13 | 1.67 | 21.17 | 0.00 | 0.00 | 0.61 | 0.40 | 0.06 | 0.03 | 0.00 | 0.00 | 0.00 | 0.00 |
| $K_2O$ | 0.63 | 19.90 | 0.45 | 0.61 | 15.10 | 18.29 | 1.56 | 26.73 | 0.51 | 11.24 | 27.29 | 11.26 | 11.45 | 13.45 | 25.98 | 1.52 | 22.33 |
| Total | 100.00 | 99.99 | 100.00 | 100.00 | 99.99 | 100.01 | 100.00 | 99.80 | 99.91 | 95.96 | 99.99 | 94.99 | 94.99 | 99.81 | 99.92 | 100.00 | 99.97 |
| Formula ratio per given O | | | | | | | | | | | | | | | | | |
| *O* | 12 | 24 | 12 | 12 | 24 | 24 | 12 | 9 | 5 | 11 | 9 | 11 | 11 | 32 | 9 | 5 | 24 |
| Si | 3.052 | 8.658 | 3.014 | 3.023 | 8.519 | 8.433 | 3.040 | 3.993 | 1.024 | 3.468 | 3.948 | 3.490 | 3.465 | 7.939 | 3.975 | 1.076 | 9.563 |
| Al | 1.978 | 3.056 | 1.950 | 1.975 | 3.470 | 3.260 | 1.965 | 0.047 | 1.951 | 2.012 | 0.055 | 1.976 | 2.040 | 9.654 | 0.092 | 1.881 | 1.881 |
| Mg | 1.400 | 0.202 | 1.566 | 1.712 | 0.406 | 0.326 | 1.270 | 0.001 | 0.017 | 0.531 | 0.031 | 0.575 | 0.522 | 0.000 | 0.000 | 0.000 | 0.000 |
| Ca | 1.501 | 0.082 | 1.459 | 1.252 | 0.019 | 0.256 | 1.631 | 0.000 | 0.000 | 0.043 | 0.024 | 0.004 | 0.002 | 0.000 | 0.000 | 0.000 | 0.000 |
| K | 0.057 | 3.633 | 0.041 | 0.055 | 2.665 | 3.327 | 0.143 | 1.882 | 0.018 | 0.943 | 1.933 | 0.953 | 0.970 | 3.204 | 1.816 | 0.052 | 4.094 |
| Total | 7.988 | 15.631 | 8.031 | 8.017 | 15.079 | 15.601 | 8.049 | 5.924 | 3.009 | 6.997 | 5.991 | 6.999 | 7.000 | 20.797 | 5.883 | 3.009 | 15.538 |
| $Al^{IV}$ | | | | | | | | | | | | | | | | | |
| $Al^{VI}$ | | | | | | | | | | | | | | | | | |
| $Mg^{M1}$ | | | | | | | | | | | | | | | | | |
| $Mg^{M2}$ | | | | | | | | | | | | | | | | | |
| $X_{Ca}^{Grt}$ | 0.517 | | 0.476 | 0.414 | | | 0.536 | | | | | | | | | | |

[a]Garnet present in the sample is not analyzed because of size of grains
[b]Probably contaminated with *SWd*
[c]*Q* denotes phases formed by quenching of the alumino-silicate glass

The most potassium-rich clinopyroxene crystals (4.5–5.62 wt% of $K_2O$) were found near the solidus (1,200–1,300 °C) (runs 688, 869, 940; Tables 1 2, 3, 4). These crystals are slightly zoned (Fig. 2c): contents of both $K_2O$ and $Al_2O_3$ systematically decrease from core to rim. However, variations of $K_2O$ within the individual crystals are weak. For example, the $K_2O$ content of the crystal from sample 688 studied by Bindi et al. (2002) varies within 4.98–5.04 wt%. Such systematic zoning implies that the crystallization of *KCpx* starts from higher $K_2O$ content and subsequently has been equilibrated during the experiment.

The important compositional relationships of high-potassic clinopyroxene are discovered in run 869 (Table 1), in which high-potassic clinopyroxene (up to 5.6 wt% of $K_2O$) coexists with *Grt* and *SWd*. In addition to *KCpx*, another clinopyroxene-like phase is observed in the sample. The phase forms euhedral crystals similar to *KCpx*. However, its composition (a.f.u. per six oxygen atoms) in comparison with the *KCpx* with the maximal $K_2O$ content is different.

This phase shows a direct correlation between K and Si. Evidently, such correlation is related to the presence of the excess K-silicate, i.e., *SWd*, as sub-microscopic inclusions in *KCpx*. The admixture of *SWd* in *KCpx* in sample 869 is related to equilibrium of *SWd* with the Al-rich *KCpx* solid solution (see discussion below).

The synthesized *KCpx* show the following uniform compositional characteristics and crystal chemical features (Tables 2, 3, 4, Fig. 5 a–c):

1. Potassium shows direct correlation with $Al^{VI}$–$Al^{IV}$, accounting for the Ca-Tschermack component (Fig. 5a), but negative correlation with Ca (Fig. 5b). This strongly suggests the isomorphic scheme $Mg^{M1} + Ca^{M2} \Leftrightarrow Al^{M1} + K^{M2}$. Deviation of the data points from the theoretical correlation lines suggests a presence of an excess Al in the M1 site and vacancies in the M2 site.
2. The excess of Al in the M1 site (e.g. $Al^{VI}$–K–$Al^{IV}$) and its direct correlation (at a ratio 2:1) with vacancies in the M2 site, e.g. $\square = 1\text{-Ca–K-}Mg^{M2}$, for most clinopyroxenes (Fig. 5c), is good evidence for the Ca-Eskola component ($Ca_{0.5}\square_{0.5}AlSi_2O_6$) in the clinopyroxene solid solution.
3. Clinopyroxenes are characterized by low Al content in the tetrahedral site ($Al^{IV} = 2\text{-Si}$) that corresponds to insignificant concentration of the Ca-Tschermack component ($CaAl_2SiO_6$). The maximum $Al^{IV}$ content (0.16–0.17 f.u.) is observed for clinopyroxenes crystallized at high temperatures in the garnet-free assemblages.
4. Low Mg content in the M2 site reflects low enstatite content in clinopyroxenes.

The *KJd* content in *KCpx* varies with temperature (Fig. 6). In order to illustrate the dependence on temperature, we took compositions of *KCpx* synthesized at 60 mol% of $KAlSi_2O_6$ in the starting mixture, since this mixture produced the best euhedral compositionally homogeneous crystals. At temperatures between 1,600

| Phase | Si | Al | Mg | Ca | K |
|---|---|---|---|---|---|
| *KCpx* | 1.994 | 0.302 | 0.705 | 0.725 | 0.258 |
| *KCpx*-like phase | 2.188 | 0.312 | 0.412 | 0.430 | 0.628 |

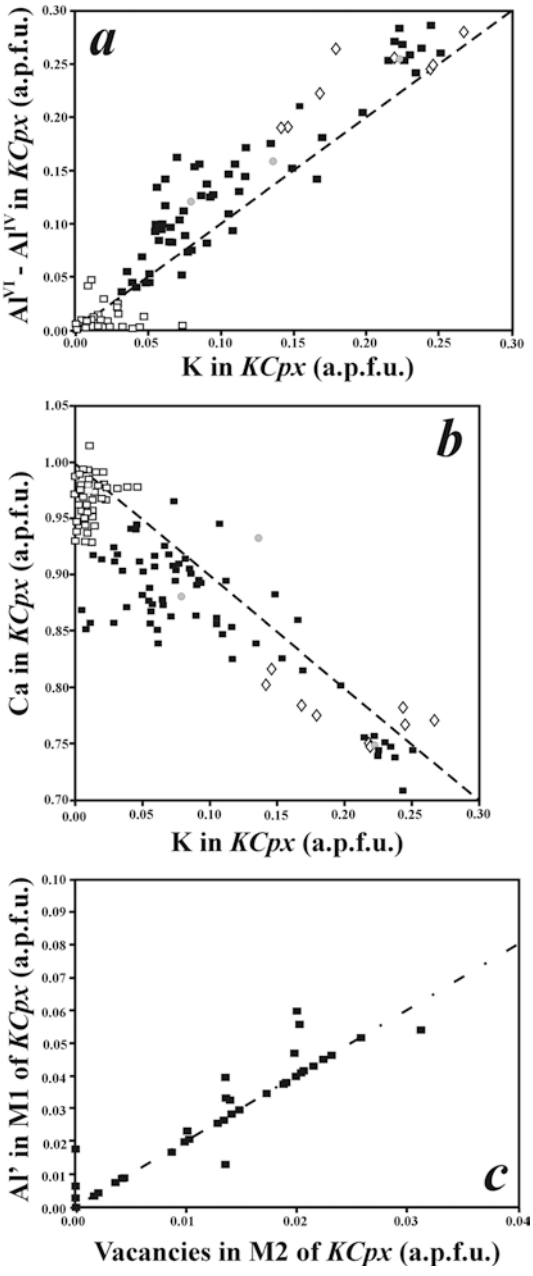


**Fig. 5** Compositional variations in *KCpx,* synthesized in the system $CaMgSi_2O_6$–$KAlSi_2O_6$ at 7 GPa (*filled rectangles*), in comparison to the previous data on Al-bearing *KCpx* produced in the carbonate-silicate systems by Chudinovskikh et al. (2001) (*empty rhombs*) and Matveev et al. (1998) (*filled circles*). **a** Positive correlation of K with $Al^{VI}$–$Al^{IV}$ (i.e., accounting for the Ca-*Ts* component); **b** negative correlation of K with Ca. **c** Correlation of the excess Al' in the M1 site with vacancies in the M2 site. *Empty rectangles* show the analysis of *Cpx* contaminated by *SWd* (excess K over Al) from *Di*-rich portion of the system. *Dashed lines* in **a** and **b** reflect the theoretically coupled heterovalent isomorphism $Mg^{M1} + Ca^{M2} \Leftrightarrow Al^{M1} + K^{M2}$ in the binary solid solution *Di-KJd. Centered line* in **c** reflects the theoretically coupled heterovalent isomorphism $Mg^{M1} + 0.5Ca^{M2} \Leftrightarrow Al^{M1} + K^{M2}$ in the binary solid solution *Di*-Ca-*Esk*

and 1,550 °C, the equilibrium *KJd* content of *KCpx* ranges from 7 to 10 mol%. The *KJd* content of 17–21 mol% is observed at a temperature of 1,300 °C,

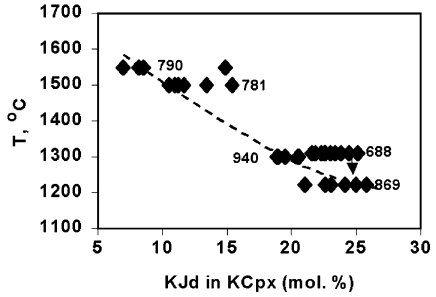


**Fig. 6** Variation of the *KJd* content with temperature for *KCpx* synthesized in the system $CaMgSi_2O_6$–$KAlSi_2O_6$ at 60 mol.% of $KAlSi_2O_6$ in the system. Labels at every group of data points indicate run numbers in Table 1. An *arrow* at the data points of the run 688 indicates that the final temperature of this run is 50 °C lower than the starting temperature (see Table 1)

whereas the *KJd* content increases 22–26 mol% at the solidus of the system (1,200–1,250 °C). The *KCpx* = *KCpx* + *L* boundary in Fig. 4 is drawn using these ranges of *KCpx* compositions (bars in Fig. 4). Preliminary runs at a temperature below 1,100 °C showed no high potassium content in clinopyroxenes. Two possible reasons can explain this feature: (1) sluggish kinetics at low temperatures and (2) exsolution of the *KCpx* below the solidus (i.e., at a possible solvus).

*Garnet* All garnets of run products are characterized by high grossular content that varies within 40–60 mol% (Tables 2, 3, 4). A conspicuous feature of some garnet compositions is an excess of Si and K in formulas (Tables 2, 3, 4). This is accompanied by a deficiency of cations in the eight-fold site (i.e., Ca + Mg < 3) and aluminum in the octahedral site. An excess of potassium in the garnet formula shows very weak positive correlation with the excess of Si and negative correlation with the run temperature. These compositional peculiarities could correspond to either contamination with *SWd* or K-fluorescence during the microprobe analysis.

*Kalsilite* The single-crystal XRD study of kalsilite in the run products is impossible because of the grain size problem. In the $KAlSi_2O_6$-rich portion of the system rare potassium-bearing crystals with Si:Al ratio close to 1 are likely hexagonal kalsilite, suggested from the powder XRD examination. However, this phase shows a systematic widely varied deficiency of potassium, whose content rarely reaches 8 a.f.u. per 32 oxygens (Tables 2, 3, 4). This deficiency of K could result from a loss of this component under the electron beam during analysis. However, a negative correlation between Si and Al is observed in this phase. In addition, the higher the silica contents in the phase the stronger the deficiency of K. These relationships may correspond to the $K + Al \Leftrightarrow \square + Si$ substitution.

*Si-wadeite* The composition of *SWd* is close to the ideal formula $K_2Si_4O_9$ (Tables 2, 3, 4). Negative correlations of potassium with Ca + Mg, as well as $Si^{VI}$

with Al, are characteristics of this phase reflecting the isomorphic substitutions $2\,K \Leftrightarrow (Ca + Mg)$ and $K + Si \Leftrightarrow (Ca, Mg) + Al$.

*Kyanite* The composition of this phase is close to the ideal formula $Al_2SiO_5$ (Tables 2, 3, 4). Slight excess of K and Si corresponds to a contamination with *SWd*.

*Alumino-silicate glass* The alumino-silicate glass in all run products is characterized by narrow, 60–62 wt% (Tables 2, 3, 4), variation of $SiO_2$ and low CaO content (< 2 wt%). In the $KAlSi_2O_6$-poor samples, the glass contains 14–16 wt% of $Al_2O_3$, 11–14 wt% of $K_2O$, 8–10 wt% of MgO (Tables 2, 3, 4). In contrast to the $KAlSi_2O_6$-poor samples, the $KAlSi_2O_6$-rich samples (*KCpx*-free) show an increase of $Al_2O_3$ and $K_2O$ contents in the glass up to 18–20 and 19–21 wt%, respectively. In turn, the glass in these samples is appreciably depleted in MgO (< 2 wt%). At pure $KAlSi_2O_6$ and a temperature of 1,650 °C, the glass is close to the leucite composition. The glass composition also varies with temperature. In the potassium-poor samples, the $KAlSi_2O_6$ content in the glass increases from 50–60 mol% at 1,600 °C, and up to 80 mol% close to the solidus (~1,300 °C). In the potassium-rich samples, the $KAlSi_2O_6$ content in the glass decreases (within the narrow interval 90–100 mol%) with the decrease of temperature. In general, composition of alumino-silicate glasses from all run products lies close to the *Di*-"*Lc*" join and is not beyond the compositional region defined by major phases in the system. It implies no peritectic relations in the system (Fig. 4).

There are two groups of phases which are considered to be products of quenching of the alumino-silicate glass. The first group includes phases, whose composition is close to K-feldspar (see Tables 2, 3, 4, samples 790 and 650). The second group consists of Mg-bearing phases (up to 5–6 wt% of MgO) with low total of oxides (about 95 wt%). Evidently, these are hydrous phases, whose formation is related to the presence of some amount of water in the starting mixtures. Composition of these phases is close to that of silica-rich phengitic micas (see Tables 2, 3, 4, samples 683, 863, and 870). The isomorphism $2Al \rightarrowtail Mg + Si$ is evident in these phases.

## Discussion and application to natural assemblages

At a pressure of 7 GPa, in the system with $KAlSi_2O_6$ of up to 60 mol%, *KCpx* is the liquidus phase, being crystallized prior to other phases. This agrees with the observations of *KCpx* in natural rocks. This mineral commonly forms inclusions in different high-pressure minerals, such as diamonds from kimberlites (e.g., Harlow and Veblen 1991; Stachel et al. 2000) and garnets (e.g., Sobolev and Shatsky 1990; Perchuk et al. 1996) from the Kokchetav UHP rocks. This implies that *KCpx* could have crystallized at the earliest stages of rock evolution, being a precursor to some other high-pressure minerals. For example, Perchuk and Yapaskurt (1998) and Perchuk et al. (2002) suggested that *KCpx* inclusions in garnets from garnet-clinopyroxene rocks of the Kokchetav Complex indicate that the *KCpx* with 1.2 wt% was crystallized at the liquidus of a K-rich liquid.

Previously, Harlow (1999) obtained clinopyroxene with 3.76 wt% of $K_2O$ in the system *Cpx*-*Kfs* at a pressure of 9.5 GPa, that was the maximal potassium content in clinopyroxene from alumino-silicate systems. Our systematic study of the system $CaMgSi_2O_6$–$KAlSi_2O_6$ showed that depending on the temperature the *KCpx* could contain up to 5.62 wt% of $K_2O$ (Tables 2, 3, 4). *KCpx* with close $K_2O$ content (4.7–5.75 wt% of $K_2O$) were reported for the carbonate-silicate systems (Harlow 1997; Matveev et al. 1998; Chudinovskikh et al. 2001).

The mechanism of potassium entry in *KCpx* is based on the substitution $K^{M1} + Al^{M2} \rightarrowtail Ca^{M1} + Mg^{M2}$ (Fig. 5a, b) supporting the idea of a presence of the potassium jadeite (*KJd*) end-member in the clinopyroxene solid solution (e.g., Harlow 1996; Perchuk et al. 1995, 1996; Chudinovskikh et al. 2001). The crystal chemistry of the produced clinopyroxenes is comparable with that of Al-bearing clinopyroxenes from the carbonate-silicate systems (Matveev et al. 1998; Chudinovskikh et al. 2001). According to Fig. 5a, *KCpx* from both the alumino-silicate and carbonate-silicate systems are characterized by a low content of $Al^{IV}$, i.e., low Ca-*Ts* content. Only some high-temperature clinopyroxenes in *Grt*-free assemblages contain notable $Al^{IV}$, because of the reaction

$$2Grs + Prp \Rightarrow 3Di + 3\mathrm{Ca}{-}Ts \qquad (8)$$

that is shifted with temperature to the right side.

Nevertheless, *KCpx* always shows an excess of $Al^{M1}$ with respect to K or *KJd* (Fig. 5a, c). Coupled with low Ca-*Ts* content, this excess corresponds to the presence of the Ca-*Esk* component in the solid solution. Experimental data indicate that the Ca-*Esk* is a characteristic end-member of high-pressure clinopyroxenes that crystallize from $SiO_2$-saturated environments (Khanukova et al. 1976; Gasparik and Lindsley 1980). Thus, the presence of the Ca-*Esk* in *KCpx* indicates high activity of $SiO_2$ in coexisting melts. Harlow (1999) and Chudinovskikh et al. (2001) paid attention to the positive influence of the Ca-*Esk* on the solubility of $K_2O$ in *KCpx*. Harlow (1999) showed that natural *KCpx* containing Ca-*Esk* show higher *KJd* content (in contrast to Ca-*Ts*-rich clinopyroxenes). Chudinovskikh et al. (2001) suggested that the vacancies in M2 provoke local relaxations in the clinopyroxene structure, assisting the incorporation of large potassium ion. At high $K_2O$ concentration (above 5 wt%), the Ca-*Esk* was found to be absent in clinopyroxene, while the pyroxenoid-structured domains (wollastonite) were documented by the Raman spectroscopy (Chudinovskikh et al. 2001). In clinopyroxenes of the $CaMgSi_2O_6$-$KAlSi_2O_6$ system, we do not observe such compositional variations. High-K

*KCpx* contain the Ca-*Esk* (Fig. 5a, c). The presence of the pyroxenoid-like domains was not inferred from the XRD single-crystal study of *KCpx* (Bindi et al. 2002).

Presumably, the structural modifications of *KCpx* (Bindi et al. 2002) control both the maximal solubility of potassium in clinopyroxene and/or the field of its stability. This is still a problem whether 5.62 wt% is the maximal $K_2O$ content for Al-rich clinopyroxene in the studied system, or not. From the relationships of *KCpx*, *Grt* and *SWd* in the run products we may assume that this content is very close to the maximal value at the experimental parameters used. According to the phase diagram of Fig. 4, at $KAlSi_2O_6$ above 75 mol% in the system, no *KCpx* is present in the solidus, while the grossular-rich garnet (up to 50 mol% of grossular) is stable between 75 and, probably, 90 wt% of $KAlSi_2O_6$. The following reaction is assumed to establish a boundary between *KCpx* solid solution and *Grt* + *SWd* assemblage in the phase diagram of Fig. 4:

$$4KJd + 3Di = Grs + Prp + 2SWd \quad (9)$$

i.e., $KCpx_{ss} = Grt_{ss} + 2SWd$. The reaction (9) shifts to the right side with an increase of *KJd* in clinopyroxene. Above a maximal limit of *KJd* (at given P and T) we can expect the decomposition (exsolution) of *KCpx* to form *SWd* and *Grt*. The formation of such admixture of K-silicate in high-potassic *KCpx* is identified in the sub-solidus run 869 (Table 1). Therefore, the reaction (9) cuts off an unstable right branch of a "solvus" of the *Di-KJd* solid solution. The left branch of this "solvus" (Fig. 4) shows the maximal solubility of the *KJd* end member in the stable *KCpx* solid solution at constant T and P. Tsuruta and Takahashi (1998) observed the coexistence of two *KCpx* with different $K_2O$ contents (0.84 wt% of $K_2O$ vs. 1.65 wt% of $K_2O$) in the solidus of potassium-rich basalt at 6 and 7 GPa. These relations also could correspond to equilibrium of *KCpx* within solvus. In our case, high-potassic *KCpx* is unstable owing to reaction (9), and the assemblage *KCpx* + *Grt* + *SWd* forms inside the "solvus" curve instead of two coexisting *KCpx*. The maximal *KJd* content of ~26 mol% in *KCpx* from sample 869 (Tables 2, 3, 4) suggests that this concentration of $K_2O$ is close to the maximal value for the clinopyroxene at given *P–T* parameters. This is in a full agreement with the conclusions of Chudinovskikh et al. (2001) for the carbonate-silicate system at similar pressure.

The *Grs* content of garnets from both the model (e.g., Luth 1997; Harlow 1999, 2002) and natural Al-Si systems (Edgar and Vukadinovic 1993; Mitchell 1995; Edgar and Mitchell 1997; Tsuruta and Takahashi 1998; Wang and Takahashi 1999) does not exceed 25 mol%, while in the potassium-rich carbonate-silicate systems it reaches about 50 mol%. (Matveev et al. 1998; Chudinovskikh et al. 2001). Grossular-rich *Grt* (40–60 mol% of *Grs*) is stable in the whole compositional interval of the $CaMgSi_2O_6$-$KAlSi_2O_6$ system. Its appearance is determined by the initial ratio Ca/Mg ~1.0 fixed by *Di*. The equilibrium between the assemblage of Ca-rich garnet with *KCpx* and potassium-rich alumino-silicate melt can be expressed

$$\underset{Grt}{\{Ca_3Al_2Si_3O_{12}+Mg_3Al_2Si_3O_{12}\}} + \underset{L}{\{2K_2O + 8SiO_2\}} = \underset{KCpx}{\{3CaMgSi_2O_6+4KAlSi_2O_6\}} \quad (10)$$

Tables 2, 3, and 4 show that both minerals coexist with the melt containing up to 62 wt% of silica at about 15 wt% of $K_2O$.

The K-silicate, *SWd*, is a common product of our experiments (Fig. 4). *SWd* is present in most of model experimental systems, both alumino-silicate (e.g., Harlow 1999) and carbonate-silicate (Harlow 1997; Matveev et al. 1998; Chudinovskikh et al. 2001). However, until now *SWd* was never observed in natural rocks, as well as in experiments with natural starting materials (e.g., K-rich lamproites). This phase was not observed in the system diopside–phlogopite (Luth 1997), which was characterized by the presence of forsterite. In contrast, *SWd* readily coexists with enstatite (higher $SiO_2$ content) and high-potassium *KCpx* (up to 3.76 wt% $K_2O$) in the *Di—Kfs* system (Harlow 1999). All these observations indicate that the formation of *SWd* is a result of simultaneously high $K_2O$ and $SiO_2$ activities in the melt. The positive influence of these parameters on potassium content in clinopyroxene was previously suggested from the analysis of the *KCpx*/melt equilibria (Perchuk et al. 2002). Thus, these observations show that the formation of the above assemblage is related to crystallization of melts that are relatively rich both in potassium and silica. Such melts are known from inclusions in diamonds. The $K_2O$ content of the inclusions, 13–16 wt% (Navon et al. 1988; Schrauder and Navon 1994; Novgorodov et al. 1990), is close to the $K_2O$ content of the alumino-silicate melts produced in our experiments in equilibrium with *KCpx*. However, silica and alumina contents of the melt inclusions in diamonds widely vary from 45–50 wt% and ~10 wt% (Navon et al. 1988; Schrauder and Navon 1994) up to 61–64 wt% and 14–18 wt% (Novgorodov et al. 1990). The composition of the first group of inclusions resembles the composition of melts produced along with *KCpx* in the phlogopite-bearing experiments (Luth 1997; Harlow 2002), whereas composition of the second group of inclusions closely corresponds to the composition of melts equilibrated with *KCpx* in the *Cpx-Kfs* (Harlow 1999) and our present experiments.

## Conclusions

We have performed the first experimental study of melting relations of the pseudo-binary system $CaMgSi_2O_6$–$KAlSi_2O_6$ at 7 GPa and presented the general topology of phase diagram involving potassium-bearing clinopyroxene

solid solution. The experiments confirmed an ultra-high solubility (up to 26 mol%) of potassium end-member, $KAlSi_2O_6$, in high-pressure Fe-free clinopyroxene from the alumino-silicate systems. The results clearly demonstrate that clinopyroxene can be an unmatched container of potassium at depths of about 200 km. A possibility of the formation of ultra-high potassic *KCpx* agrees with very recent finding of natural *KCpx* with 3.6 wt% of $K_2O$ (Bindi et al. 2003). At shallower depths *KCpx* dramatically loses potassium. However, even at pressures of about 5 GPa we could expect the $K_2O$ concentration of 1.0–1.5 wt% in *KCpx*, which are characteristic for some natural mantle clinopyroxenes. Potassium, released by *KCpx* at decompression, easily escapes into coexisting melts or fluids. Such potassium-rich liquids are known to be the most active agents of mantle magmatism and metasomatism.

**Acknowledgements** Constructive personal discussions with George Harlow and Andrey Girnis gave some new ideas to the interpretation of the experiments and phase diagram. Comments by Robert Luth, Roland Stalder, and Mario Tribaudino improved the text of the paper. Authors especially thank J. Hoefs and J. Touret for quick organization the paper review. The authors are very grateful to Ludmila P. Red'kina (Institute of Experimental Mineralogy) for the preparation of starting materials and mixtures. The facilities for electron microprobe analyses were provided by both the Department of Petrology (analysts Elena V. Guseva and Natalia N. Korotaeva) and the Department of Mineralogy (analyst Dmitriy A. Varlamov) of the Moscow State University. This study is supported by the Russian Foundation for Basic Research (projects 01-05-64775, 03-05-06289 to OGS and 02-05-64684 to Y.A.L.), the program for young scientists of the Russian Academy of Science (project no. 323 to O.G.S.), the Science Support Foundation (program for young scientists), the Russian State Leading Scientific Schools Program (project no. 16452003.5 to L.L.P.), and by M.U.R.S.T., cofinanziamento 2001, project "Structural complexity and properties of minerals: microstructures, modularities, modulations" (to L.B. and S.M.).

## Abbreviations

Mineral abbreviations

| | |
|---|---|
| Ca-Esk | Ca-Eskolaite ($Ca_{0.5}AlSi_2O_6$) |
| Ca-Ts | Ca-Tschermackite ($CaAl_2SiO_6$) |
| Cpx | potassium-free clinopyroxene solid solution |
| Di | diopside ($CaMgSi_2O_6$) |
| Fo | forsterite ($Mg_2SiO_4$) |
| $G_S$ | alumino-silicate glass |
| Grs | grossular ($Ca_3Al_2Si_3O_{12}$) |
| Grt | garnet solid solution |
| KCpx | potassium-bearing clinopyroxene solid solution |
| Kfs | K-feldspar ($KAlSi_3O_8$) |
| KJd | potassium jadeite ($KAlSi_2O_6$) |
| Ks | kalsilite ($K_8Al_8Si_8O_{32}$, the formula $KAlSiO_4$ is used in the reactions in the text for simplicity) |
| Ky | kyanite ($Al_2SiO_5$) |
| L | alumino-silicate melt |
| Lc | leucite ($KAlSi_2O_6$) |
| Mc | mica-like phases, quench products of the alumino-silicate melt |
| Prp | pyrope ($Mg_3Al_2Si_3O_{12}$) |
| Q | quench products of the alumino-silicate melt |
| SWd | Si-wadeite ($K_2Si_4O_9$) |

## References

Bindi L, Safonov OG, Litvin YA, Perchuk LL, Menchetti S (2002) Ultrahigh potassium content in the clinopyroxene structure: an X-ray single-crystal study. Eur J Mineral 14:929–934

Bindi L, Safonov OG, Yapaskurt VO, Perchuk LL, Menchetti S (2003) Ultrapotassic clinopyroxene from the Kumdy-Kol microdiamond mine, Kokchetav Complex, Kazakhstan: occurrence, composition and crystal-chemical characterization. Am Mineral 88:464–468

Bishop FC, Smith JV, Dawson JB (1978) Na, K, P and Ti in garnet, pyroxene and olivine from peridotite and eclogite xenoliths from African kimberlites. Lithos 11:155–173

Bowen NL, Schairer JF (1929) The system leucite-diopside. Am J Sci, 5th ser. 18:301

Bradley CC (1969) High-pressure methods in solid-state research. Butterworths, London

Chudinovskikh LT, Zharikov VA, Ishbulatov RA, Matveev YA (2001) On the mechanism of incorporation of ultra-high amounts of potassium into clinopyroxene at high pressure. Dokl Rossikoi Akad Nauk, Earth Sci 380:1-4

Edgar AD, Mitchell RH (1997) Ultra high pressure-temperature melting experiments on an $SiO_2$-rich lamproite from Smoky Butte, Montana: derivation of siliceous lamproite magmas from enriched sources deep in the continental mantle. J Petrol 38:457–477

Edgar AD, Vukadinovic D (1993) Potassium-rich clinopyroxene in the mantle: an experimental investigation of K-rich lamproite up to 60 kbar. Geochim Cosmochim Acta 57:5063–5072

Fasshauer DW, Wunder B, Chatterjee ND, Höhne GWH (1998) Heat capacity of wadeite-type $K_2Si_4O_9$ and pressure-induced stable decomposition of K-feldspar. Contrib Mineral Petrol 131:210–218

Gasparik T (1996) Melting experiments on the enstatite-diopside join at 70–224 kbar, including the melting of diopside. Contrib Mineral Petrol 124:139–153

Gasparik T, Lindsley DH (1980) Experimental study of pyroxenes in the system $CaMgSi_2O_6$–$CaAl_2SiO_6$–$Ca_{0.5}AlSi_2O_6$. EOS 61:402–403

Gasparik T, Litvin YA (1997) Stability of $Na_2Mg_2Si_2O_7$ and melting relations on the forsterite-jadeite join at pressures up to 22 GPa. Eur J Mineral 9:311–326

Ghorbani MR, Middlemost EAK (2000) Geochemistry of pyroxene inclusions from the Warrumbungle Volcano, New South Wales, Australia. Am Mineral 85:1349–1367

Hamilton DL, Henderson CMB (1968) The preparation of silicate compositions by a gelling method. Mineral Mag 36:832–838

Harlow GE (1996) Structure refinement of a natural K-rich diopside: the effect of K on the average structure. Am Mineral 81:632–638

Harlow GE (1997) K in clinopyroxene at high pressure and temperature: an experimental study. Am Mineral 82:259–269

Harlow GE (1999) Interpretation of KCpx and CaEs in clinopyroxene from diamond inclusions and mantle samples. Proc Seventh Intern Kimberlite Conf, vol **I**, Cape Town, South Africa

Harlow GE (2002) Diopside + F-rich phlogopite at high P and T: Systematics, crystal chemistry and stability of $KMgF_3$, clinohumite and chondrodite. Geol Mater Res 4(3):1–28

Harlow GE, Veblen DR (1991) Potassium in clinopyroxene inclusions from diamonds. Science 251:652–655

Homan CG (1975) Phase diagram of Bi up to 140 kbars. J Phys Chem Solids 36:1249–1254

Jaques AL, O'Neill HSC, Smith CB, Moon J, Chappell BW (1990) Diamondiferous peridotite xenoliths form the Argyle (AK1) lamproite pipe, Western Australia. Contrib Mineral Petrol 104:255–276

Kennedy CS, Kennedy GC (1976) The equilibrium boundary between graphite and diamond. J Geophys Res 81:2467–2470

Khanukova LT, Zharikov VA, Ishbulatov RA, Litvin YA (1976) Excess silica in solid solutions of high-pressure clinopyroxenes as shown by experimental study of the system $CaMgSi_2O_6$-$CaAl_2SiO_6$-$SiO_2$ at 35 kilobars and 1,200 °C. Dokl Akad Nauk SSSR Earth Sci 229:170–172

Litvin YA (1990) Physical and chemical studies of melting of materials from the deep earth (in Russian). Nauka Press, Moscow

Liu L (1987) High-pressure transition of potassium aluminosilicates with an emphasis on leucite. Contrib Mineral Petrol 95:1–3

Luth RW (1992) Potassium in clinopyroxene at high pressure: experimental constraints. EOS Trans Am Geophys Un 73:608

Luth RW (1995) Potassium in clinopyroxene at high pressure. EOS Trans Am Geophys Un 76: F711

Luth RW (1997) Experimental study of the system phlogopite-diopside from 3.5 to 17 GPa. Am Mineral 82:1198–1209

Maaløe S (1985) Principles of igneous petrology. Springer, Berlin Heidelberg New York

Matveev YA, Litvin YA, Perchuk LL, Chudinovskikh LT, Yapaskurt VO (1998) Intensive carbonate-silicate reactions in the $K_2Mg(CO_3)_2$–$(Ca_{0.5}Mg_{0.5})SiO_3$–$Al_2O_3$ system in experiment at 7 GPa: relation to Kokchetav-type diamond deposits. Terra nova v. 10, Terra Abstr, Suppl 1:39

McCandless TE, Gurney JJ (1986) Sodium in garnet and potassium in clinopyroxene: criteria for classifying mantle eclogites. Blackwell, Victoria, Geol Soc Aust Spec Publ 14:827–832

McGregor ID, Carter JL (1970) The chemistry of clinopyroxenes and garnets of eclogite and peridotite xenoliths from the Roberts Victor mine, South Africa. Phys Earth Planet Inter 3:391–397

Mitchell RH (1995) Melting experiments on a sanidine-phlogopite lamproite at 4–7 GPa and their bearing on the source of lamproitic magmas. J Petrol 36:1455–1474

Moore JD, Gurney JJ (1985) Pyroxene solid solution in garnets included in diamond. Nature 318:582–584

Navon O, Hitcheon ID, Rossman GR, Wasserburg GJ (1988) Mantle-derived fluids in diamond microinclusions. Nature 325:784–789

Novgorodov PG, Bulanova GP, Pavlova LA, Mikhailov VN, Ugarov VV, Shebanin AP, Argunov KP (1990) Inclusions of potassic phases, coesite and omphacite in the coated diamond crystal from the "Mir" pipe. Dokl Akad Nauk SSSR Earth Sci 310:439–443

Perchuk LL, Yapaskurt VO (1998) Mantle-derived ultrapotassic liquids. Russ Geol Geophys 39:1746–1755

Perchuk LL, Yapaskurt VO, Okay A (1995) Comparative petrology of diamond-bearing metamorphic complexes. Petrology 3:238–276

Perchuk LL, Sobolev NV, Yapaskurt VO, Shatsky VS (1996) Relics of potassium-bearing pyroxenes from diamond-free pyroxene-garnet rocks of the Kokchetav massif, northern Kasakhstan. Dokl Rossikoi Akad Nauk Earth Sci 348:790–795

Perchuk LL, Safonov OG, Yapaskurt VO, Barton JM Jr (2002) Crystal-melt equilibria involving potassium-bearing clinopyroxene as indicators of mantle-derived ultrahigh-potassic liquids: an analytical review. Lithos 60(3–4):89–111

Prinz M, Manson DV, Hlava PF, Keil K (1975) Inclusions in diamonds: garnet lherzolite and eclogite assemblages. Phys Chem Earth 9:797–815

Reid AM, Brown RW, Dawson JB, Whitfield GG, Siebert JC (1976) Garnet and pyroxene compositions in some diamondiferous eclogites. Contrib Mineral Petrol 58:203–220

Rhines FN (1956) Phase diagrams in metallurgy. McGraw-Hill, New York

Rickard RS, Harris JW, Gurney JJ, Cardoso P (1989) Mineral inclusions in diamonds from the Koffiefontein Mine. In: Geol Soc Aust Spec Publ, Blackwell Scientific, Victoria 14, pp 1054–1062

Schrauder M, Navon O (1994) Hydrous and carbonatitic mantle fluids in fibrous diamonds from Jwaneng, Botswana. Geochim Cosmochim Acta 58:761–771

Shimizu N (1971) Potassium content of synthetic clinopyroxenes at high pressures and temperatures. Earth Planet Sci Lett 11:374–380

Sobolev NV, Shatsky VS (1990) Diamond inclusions in garnets from metamorphic rocks: a new environment for diamond formation. Nature 343:742–746

Stachel T, Brey GP, Harris JW (2000) Kankan diamonds (Guinea) I: from the lithosphere down to the transition zone. Contrib Mineral Petrol 140:1–15

Swanson DK, Prewitt CT (1983) The crystal structure of $K_2Si^{VI}Si^{IV}{}_3O_9$. Am Mineral 68:581–585

Tsuruta K, Takahashi E (1998) Melting study of an alkali basalt JB-1 up to 12.5 GPa: behavior of potassium in the deep mantle. Phys Earth Planet Int 107:119–130

Urakawa S, Kondo T, Igawa N, Shimomura O, Ohno H (1994) Synchrotron radiation study on the high-pressure and high-temperature phase relations of $KAlSi_3O_8$. Phys Chem Minerals 21:387–391

Wang W, Takahashi E (1999) Subsolidus and melting experiments of a K-rich basaltic composition to 27 GPa: Implication for behavior of potassium in the mantle. Am Mineral 84:357–361